Monitoring Controlled Release of Payload from Gold Nanocages Using Surface Enhanced Raman Scattering

Limei Tian, Naveen Gandra, and Srikanth Singamaneni*

Department of Mechanical Engineering and Materials Science, Washington University in St. Louis, St. Louis, Missouri 63130, United States

ABSTRACT Novel organic and inorganic nanostructures for localized and externally triggered delivery of therapeutic agents at a target site have received immense attention over the past decade owing to their enormous potential in treating complex diseases such as cancer. Gold nanocages, a novel class of hollow plasmonic nanostructures, have been recently demonstrated to serve as carriers for the delivery of payload with external trigger such as light or ultrasound. In this article, we demonstrate that surface enhanced Raman spectroscopy (SERS) can be employed to noninvasively monitor the release of payload from these hollow plasmonic nanostructures. The large enhancement of electromagnetic (EM) field at the interior surface of these nanostructures enables us to monitor the controlled release of Raman-active cargo from nanocages. Considering that SERS can be excited and collected in near-infrared (NIR) therapeutic window, this technique can serve as a powerful tool to monitor the drug release *in vivo*, providing additional control over externally triggered drug administration.

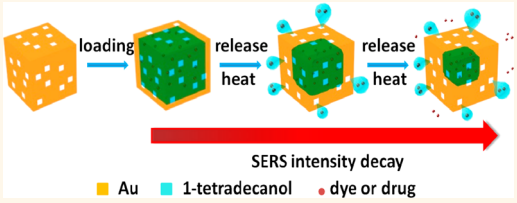

KEYWORDS: surface enhanced Raman scattering (SERS) · gold nanocages · theranostics · drug delivery · localized surface plasmon resonance

Plasmonics involves the control and confinement of light into dimensions much smaller than the wavelength of light.[1−6] The dielectrically confined oscillation of the conduction electrons in metal nanostructures with incident electromagnetic field, often termed as localized surface plasmon, renders attractive optical properties such as large absorption and scattering cross sections and large enhancement of electric field at the surface of these nanostructures.[7−10] Such plasmonic nanostructures are highly attractive for various biomedical applications including biosensing, bioimaging, photothermal therapy, and targeted drug delivery.[11−21]

Nanostructures that enable targeted and triggered release of payload (*e.g.*, chemotherapeutic drug) are ideal for administering locoregional therapy. Different classes of nanostructures including supramolecular assemblies, polymer capsules, and hollow metal nanostructures are being extensively investigated for such applications.[22−28] Gold nanocages (AuNCs), a novel class of hollow plasmonic nanostructures, is an attractive platform for theranostic applications, thanks to their highly tunable localized surface plasmon resonance (LSPR) into the near-infrared (NIR) where the endogenous absorption coefficient of living tissue is nearly two orders magnitude smaller compared to that in the visible range.[17,29] Owing to their large scattering and absorption cross sections, AuNCs have been employed as contrast agents in optical coherence tomography, photoacoustic imaging and photothermal therapy.[30−32] More recently, these hollow nanostructures have been demonstrated to be efficient carriers of chemotherapeutic drugs for targeted and triggered delivery, potentially enabling locoregional therapy and avoiding systemic toxicity of aggressive chemotherapeutic drugs. Triggered delivery of contents is achieved by heating AuNCs photothermally or ultrasonically, which in turn causes a phase change (solid−liquid or coil−globule) of the "gate keepers" such as temperature responsive polymers or biocompatible phase-change materials, resulting in the release of the contents.[33,34]

* Address correspondence to singamaneni@wustl.edu.

Received for review February 12, 2013 and accepted April 11, 2013.

Published online April 11, 2013
10.1021/nn400728t

An extremely powerful addition to this attractive drug delivery platform is the ability to remotely monitor the "drug level" within AuNCs during externally triggered drug administration. A noninvasive method for real-time monitoring of the drug delivery from these nanovehicles will provide additional handles for more efficient and controlled drug administration. Previous proof-of-concept demonstrations have relied on monitoring the absorbance of dye (employed as a model cargo) in the visible regime following its release into the solution.[34] However, considering the absence of strong absorption band in the NIR for chemotherapeutic drug molecules (*e.g.*, doxorubicin), this method cannot be used *in vitro* or *in vivo*.

Herein, we present a facile and versatile strategy for monitoring the controlled release of payload from AuNCs using surface enhanced Raman scattering (SERS). In particular, we demonstrate that SERS, which involves the dramatic enhancement of Raman scattering from molecules adsorbed on or in close proximity to a nanostructured metal surface, can serve as a noninvasive technique to monitor the release of Raman-active molecules such as dyes and drugs (*e.g.*, doxorubicin[35,36]) from plasmonic nanocages.

RESULTS AND DISCUSSION

In this study, we employed a biocompatible phase-change material (PCM), namely, 1-tetradecanol, as a "gate keeper" to control the release of cargo in response to an external stimulus, according to a recent study (Figure 1).[34] 1-Tetradecanol can reversibly change the physical state between solid and liquid at its melting point of 38−39 °C, which is slightly higher than the normal human body temperature. Furthermore, 1-tetradecanol is suitable as PCM due to its wide miscibility with many hydrophilic and hydrophobic substances, good biocompatibility, and low toxicity.[34,37] Encapsulated drugs are released along with melted 1-tetradecanol through diffusion after raising the local temperature beyond its melting point by thermal or ultrasonic means.

Synthesis and Characterization of AuNCs. Ag nanocubes were synthesized by a reported sulfide-mediated polyol synthesis method.[38] The synthesis reaction was quenched once the dipolar LSPR wavelength of the nanocubes reached ~460 nm, which yielded nanocubes with an edge length of 65 ± 5 nm (Figure 2A,B). AuNCs were obtained by galvanic replacement of Ag nanocubes with gold using $HAuCl_4$.[33] The AuNCs, which exhibited a LSPR wavelength of ~820 nm, had an outer edge length of 73 ± 5 nm and wall thickness of ~6 nm (Figure 2C,D). TEM image clearly reveals the hollow nanostructures with porous sidewalls and an average pore size of about 4 nm. The as-prepared AuNCs were concentrated in methanol after washing with nanopure water and methanol.

Monitoring Cargo Loading into AuNCs. For demonstrating SERS-based monitoring of payload release from the AuNCs, we employed nile red and doxorubicin (Dox) as model cargo. After loading the cargo (1-tetradecanol + nile red (or Dox)) into AuNCs, vis/NIR extinction spectra revealed a red shift of ~20 nm in LSPR wavelength compared to that of pristine AuNCs in aqueous suspension, which corresponds to an increase in the refractive index of the medium in and/or around the AuNCs (Figure 3A). Finite-difference time-domain (FDTD) simulations were employed to confirm the redshift in the LSPR of AuNCs upon cargo loading. The calculated extinction spectra of AuNCs with 80 nm edge length and 6 nm wall thickness exhibited two distinct plasmon bands at 802 and 710 nm. Electric vector orientations at different planes along the thickness of the AuNC reveal that the band at 802 nm corresponds to a strong dipolar resonance and the band at 710 nm is associated with a relatively weak quadrupolar resonance mode, which is in agreement with previous reports describing optical properties of spherical Au nanoshells (Figure S1, S2).[39] Enhanced electromagnetic field was observed at the corners exterior to the AuNC and adjacent to the walls on the interior surface (inset of Figure 3B). The calculated extinction spectra showed a ~12 nm red shift after

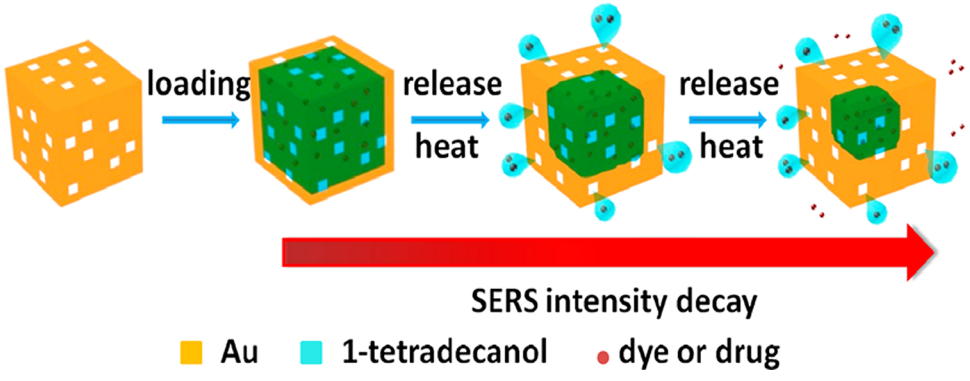

Figure 1. Scheme illustrating the loading of a gold nanocage (AuNC) with 1-tetradecanol and dye/drug followed by its release with external trigger. A decrease in the SERS intensity of dye/drug during its release can be employed to directly monitor the release process.

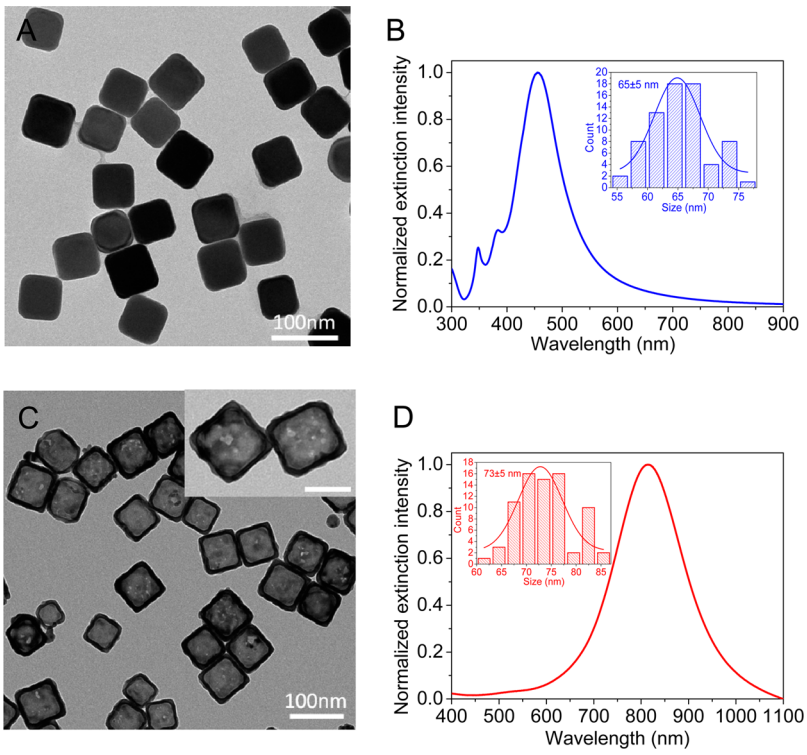

Figure 2. (A) TEM image of Ag nanocubes employed as templates for the synthesis of AuNCs. (B) UV−vis extinction spectrum of the aqueous suspension of Ag nanocubes (inset shows the histogram of the size distribution as measured from TEM images). (C) TEM image of AuNCs (inset is a high magnification image revealing the pores on the surface of walls. Scale bar corresponds to 50 nm). (D) Vis−NIR extinction spectrum of the aqueous suspension of AuNCs (inset shows the histogram of the size distribution as measured from TEM images).

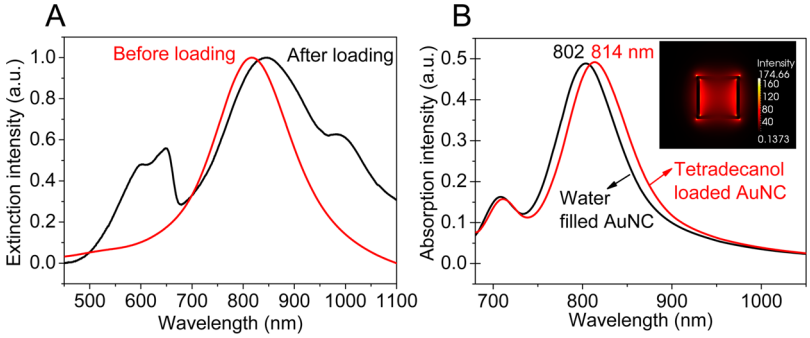

Figure 3. (A) Extinction spectra of AuNCs before and after loading the AuNCs with 1-tetradecanol and nile red. (B) Absorption spectra of AuNC obtained using FDTD simulation. The refractive index of 1-tetradecanol was assumed to be 1.44.

loading the AuNC with cargo (assuming the refractive index of cargo to be that of bulk 1-tetradecanol). Experimentally observed LSPR shift following the loading was slightly higher than that predicted by FDTD simulation possibly due to the slight aggregation of the AuNCs during the loading process, which is known to cause a red shift in LSPR wavelength (Figure 3B).[40] The loading of AuNCs with the Raman-active cargo is further confirmed by SERS spectra from AuNCs, which revealed the Raman bands corresponding to the entrapped molecules (discussed below).

Releasing Nile Red from AuNCs by Heating. Following the successful loading of the AuNCs with Raman-active cargo, we set out to demonstrate the SERS-based monitoring of the cargo release from AuNCs. Figure 4A shows the Raman spectra obtained from the individual components including 1-tetradecanol, nile red, AuNCs and AuNCs loaded with a mixture of 1-tetradecanol and nile red (Figure 4A). The most prominent bands in the SERS spectrum of AuNCs loaded with nile red are at 591 and 1642 cm^{-1}, which correspond to the ring-breathing and ethylenic-stretching vibrations of nile red, respectively.[41,42] SERS spectra were collected from individual loaded AuNCs, sparsely distributed on a poly(2-vinyl pyridine) (P2VP)-modified silicon substrate (Figure 4B and Figure S3).[43,44] Individual AuNCs were identified using an optical microscope, coupled to a Raman spectrometer, under dark field illumination (Figure 4B). For each condition, SERS spectra were collected from nearly 20 AuNCs exhibiting similar scattering

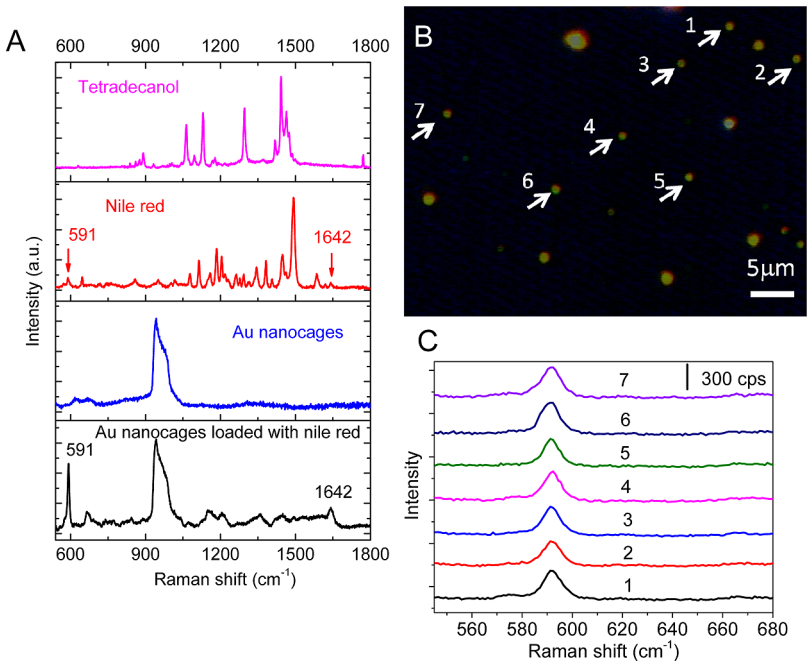

Figure 4. (A) Raman spectra of nile red and 1-tetradecanol in bulk form and AuNCs before and after loading with nile red. (B) Dark field scattering image of AuNCs loaded with nile red sparsely adsorbed on a silicon substrate. (C) Raman spectra corresponding to the marked AuNCs in panel B, which shows the remarkable spectral homogeneity of AuNCs exhibiting similar scattering intensity.

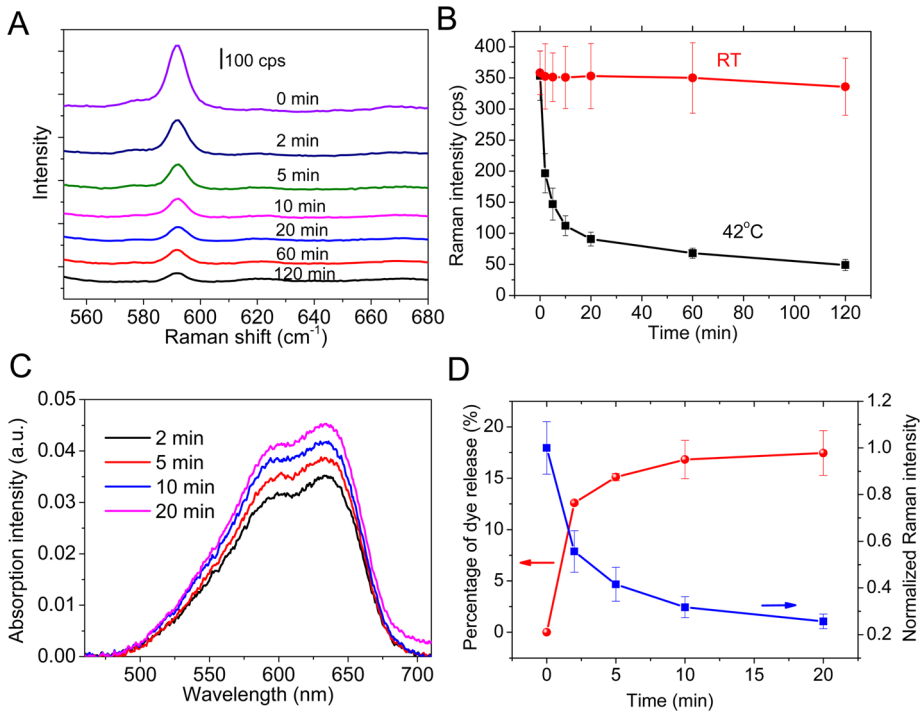

Figure 5. (A) Raman spectra of AuNCs after different durations of exposure to 42 °C water. (B) Plot showing the Raman intensity of nile red peak at 591 cm^{-1} from AuNCs exposed to water at 42 °C and water at room temperature for different durations. (C) Absorption spectra of nile red after exposure of AuNCs to 42 °C water for different durations. (D) Correlation of cargo release calculated from absorbance of nile red and change in normalized Raman intensity with time.

intensity and the average spectrum was considered for cargo release analysis. The SERS spectra obtained from individual AuNCs with similar scattering intensity exhibited remarkable spectral homogeneity both in terms of Raman peak position and intensity (RSD < 15%) (Figure 4C). The SERS enhancement factor (EF) for each AuNC at 591 cm^{-1} band was estimated to be ~2.7 × 10^6, assuming that AuNCs were filled with 1-tetradecanol and nile red with a weight ratio of 10:1 (see Supporting Information for details). The large SERS enhancement of nanocage contents spurs from the enhanced EM field adjacent to interior walls of AuNCs (inset of Figure 3B and Figure S4).

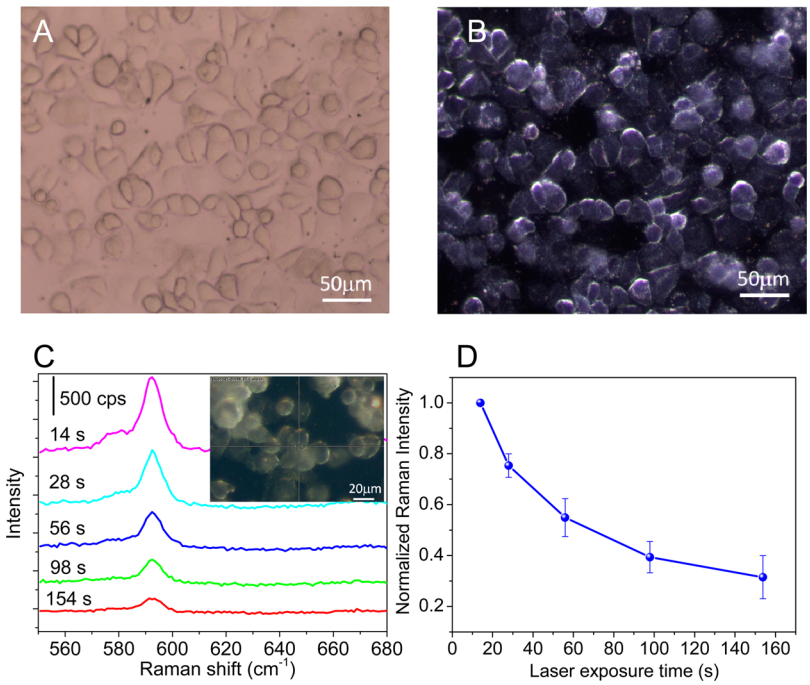

Figure 6. Optical images of SKBR3 cells incubated with AuNCs loaded with nile red under (A) bright field and (B) dark field illuminations. (C) SERS spectra of cells with loaded AuNCs, showing the release of nile red with time due to the photothermal heating of the AuNCs. (D) Decrease in SERS intensity showing the release of nile red from AuNCs in cells with increasing laser exposure time.

To monitor the release of cargo from AuNCs, SERS spectra were collected and averaged from individual AuNCs after exposure to water at 42 °C for different durations (Figure 5A). The intensity of SERS spectra exhibited a monotonic decrease in intensity with longer exposure to elevated temperature suggesting the progressive release of cargo from AuNCs (Figure 5B). On the other hand, AuNCs exposed to water at room temperature exhibited virtually no change in SERS intensity, which indicated that the nile red encapsulated by solid PCM inside AuNCs barely leaked into surrounding medium at room temperature (23 °C) (Figure 5B). The release of nile red was also probed by collecting absorption spectra of the dye released into water after exposure to 42 °C water for different durations (Figure 5C). As expected, the absorption intensity of nile red increased with increasing exposure time to elevated temperature confirming the release of nile red from AuNCs, which agreed with previous reports.[33,34] The release of payload from AuNCs, which results in a decay of Raman intensity of payload can be quantitatively calibrated by monitoring the concomitant rise in the absorption intensity of the dye released into solution (Figure 5D). A dramatic decrease in SERS intensity and increase in absorption intensity was noted within the first five minutes, which corresponds to a rapid release of the payload during this time followed by a much smaller rate subsequently. Notably, the release rate was extremely small after around 20 min with only a ~10% change in Raman intensity from 20 to 120 min.

Photothermal Release of Nile Red from AuNCs *in Vitro*. We further demonstrate the feasibility of SERS-based monitoring of the cargo release from AuNCs *in vitro* using epithelial breast cancer cells (SKBR3). SKBR3 cells seeded on poly(lysine) coated-silicon substrate were incubated with AuNCs loaded with nile red for one hour. Bright and dark field optical imaging of live cells was employed to locate the live cells for subsequent SERS measurements (Figure 6A,B). SERS spectra of the cells incubated with AuNCs were acquired using 785 nm laser with a power of ~4 mW at the sample. The rise in temperature at AuNCs' surface due to photothermal (PT) effect has been systematically examined using SERS and it was concluded that the surface temperature of AuNCs with LSPR wavelength at ~790 nm could increase the temperature by 37 °C under the excitation of 785 nm laser (laser power of 5.2 mW) under similar conditions.[45] Thus, the Raman laser induced heating of AuNCs is sufficient to melt 1-tetradecanol, which in turn results in the release of the dye from AuNCs. We observed the decrease of SERS intensity at 591 cm^{-1} with increasing laser exposure time, showing the diffusion of nile red into the surrounding medium from AuNCs due to photothermal effect (Figure 6C,D). This sensitive dependence suggests that SERS could be employed to monitor the release of cargo from AuNCs in response to external trigger such as light, heat or ultrasound.

Photothermal Release Dox from AuNCs. We also demonstrate that the release of a routinely used chemotherapeutic drug, namely, doxorubicin (Dox),[46] from AuNCs, can be monitored using SERS. Raman spectrum collected from Dox in bulk form shows several strong Raman bands, which is critical for

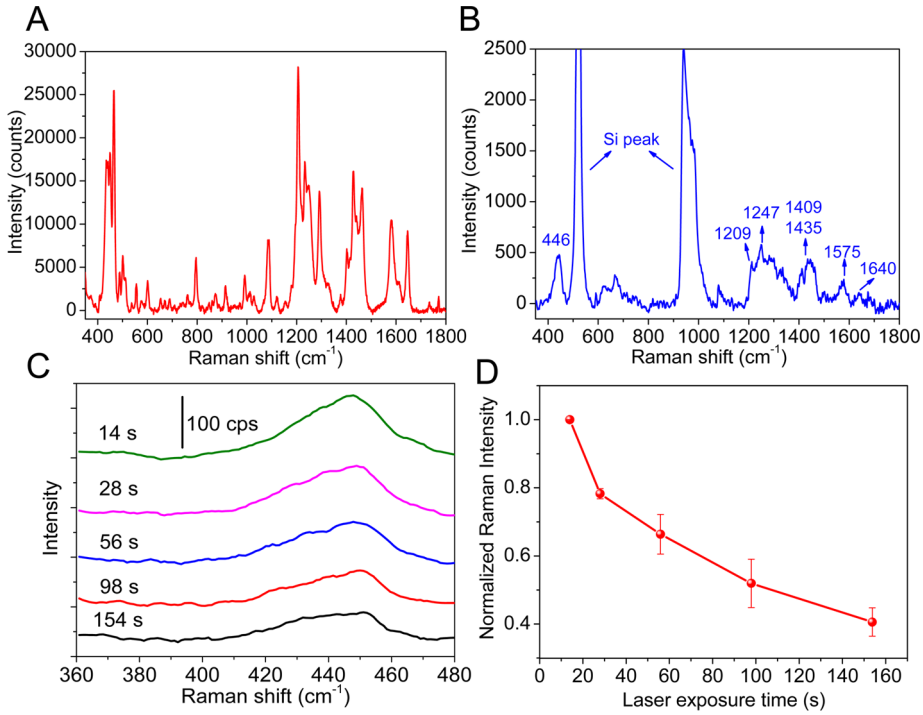

Figure 7. (A) Raman spectrum of doxorubicin (Dox) powder (bulk). (B) SERS spectra of AuNCs loaded with Dox on a silicon substrate. (C) SERS spectra of AuNCs loaded with Dox showing progressive dye release with increased laser exposure time. (D) Decay in SERS intensity of Dox-loaded AuNCs with increasing laser exposure time.

monitoring its release from AuNCs. The bands between 1200 and 1300 cm^{-1} correspond to in-plane bending motions from C−O, C−O−H, and C−H, respectively. The bands at 1409, 1435, and 1575 cm^{-1} can be attributed to the skeletal ring vibrations of Dox, and the 1640 cm^{-1} band corresponds to the hydrogen bonded C═O stretching mode (Figure 7A).[47,48] Raman spectra were collected from Dox in bulk and loaded AuNCs to confirm the encapsulation of Dox (Figure 7A, B). The most prominent band at 446 cm^{-1}, associated with the C═O in-plane deformation of Dox, was used to monitor the release of Dox from AuNCs. The decrease of SERS intensity at 446 cm^{-1} with increasing exposure time to laser showed the control release of Dox from AuNCs due to PT effect (Figure 7C,D).

While the results demonstrated here clearly show that release process can be followed *in situ* using SERS, it is not without limitation. One potential limitation in translating these results to *in vivo* settings is the limited penetration depth of NIR laser into diffuse human tissue (typically few mm).[49] However, we would like to quickly mention some recent efforts such as spatially offset SERS (SOSERS) and development of Raman endoscopes that are focused on either enhancing the depth of SERS-based bioimaging or accessing tissues, which are otherwise inaccessible with conventional Raman spectrometers.[50−52] As these techniques mature, we believe that SERS will emerge as a powerful tool for molecular bioimaging and image-guided therapy and the approach demonstrated here can form a powerful tool for monitoring controlled and externally triggered drug delivery.

CONCLUSIONS

In conclusion, we have demonstrated a simple, noninvasive and effective method for monitoring controlled release of cargo from AuNCs using SERS. The approach demonstrated here does not add any complexity to the design or fabrication of plasmonic AuNCs previously demonstrated and requires no modification to the existing loading and release procedures. Considering that SERS can be excited and collected in NIR wavelength (*e.g.*, 785 nm laser employed in this study), the approach suggested here can be potentially translated to *in vivo* settings. The simple yet powerful ability to monitor the drug release serves as a new tool for precise control over the drug administration process hinting the care provider the amount of drug released and left within the nanovehicles.

EXPERIMENTAL SECTION

Materials. Ethylene glycol (lot. no K26B01) and sodium sulfide (Na_2S) were purchased from J. T. baker. Silver nitrate (purity >99%), poly(vinyl pyrrolidone) (PVP, M_w∼29 000), chloroauric acid ($HAuCl_4$), nile red, 1-tetradecanol (97%), and methanol were obtained from Sigma-Aldrich. Poly(2-vinyl pyridine) (M_w = 200 000 g/mol) was obtained from Scientific Polymer Products. Doxorubicin (>99%) was purchased from LC

Laboratories. All the chemicals have been used as received with no further purification.

Synthesis of Silver Nanocubes. Prior to synthesis, all the glassware was cleaned using aqua regia (3:1 volume ratio of 37% hydrochloric acid and concentrated nitric acid). Silver nanocubes were synthesized using a sulfide-mediated method developed by Xia group.[33] Briefly, 80 μL of Na_2S solution (3 mM) in ethylene glycol was added to 6 mL of preheated ethylene glycol in a disposable glass vial. After 8 min, 1.5 mL of PVP (0.02 g/mL) in ethylene glycol was added to the above mixture, immediately followed by the addition of 0.5 mL of $AgNO_3$ (0.048 g/mL) in ethylene glycol. The reaction was complete in 15 min with a dark ruddy-red meniscus in reaction solution. The product was washed with acetone and water twice by centrifugation, redispersed and stored in ethylene glycol until use.

Synthesis of AuNCs. A total of 10 mL of aqueous PVP solution (9 mM) was add to 1 mL of the above-mentioned silver nanocubes solution. After bringing the suspension to a mild boil for approximately 10 min, 1 mM $HAuCl_4$ was injected at a rate of 0.5 mL/min under vigorous stirring until dark blue color appeared. The product was washed with saturated solution of NaCl to remove AgCl produced during the galvanic replacement reaction by centrifugation and redispersion in nanopure water (18.2 MΩ·cm).

Loading AuNCs with Cargo. The loading process was in accordance to a procedure previously reported with some modifications.[34] As-synthesized AuNCs (2 mL) were centrifuged and redispersed in 300 μL of methanol. Three milligrams of nile red was added to 30 mg of 1-tetradecanol at 50 °C magnetically stirred for 30 min. To this mixture, 300 μL of the above-mentioned AuNCs in methanol was added at 90 °C. The above mixture was stirred for 1 h, and then hot water was added to extract the AuNCs loaded with 1-tetradecanol and dye. Immediately, the extracted AuNCs were kept in an ice-bath for 1 min followed by centrifugation and redispersion into water to remove excess dye.

Adsorption of AuNCs Loaded with Nile Red on Silicon Surface. Silicon substrates employed for adsorbing AuNCs were cleaned using Piranha solution (3:1 concentrated sulfuric acid to 30% hydrogen peroxide solution) followed by thorough rinsing with nanopure water (*Caution: Piranha solution is extremely dangerous and proper care needs to be executed in handling and disposal.*) The silicon substrates were modified with poly(2-vinyl pyridine) (P2VP) by exposing the substrates to 1% (w/v) P2VP solution in ethanol for 1 h. Subsequently, the substrates were rinsed in copious amount of ethanol to leave an ultrathin (~1 nm) adsorbed P2VP layer. The P2VP-modified substrate was exposed to *AuNCs* solution to enable their adsorption. Finally, the substrate was rinsed with water to remove the loosely bound AuNCs and the dye residue leaving behind a sparsely dispersed AuNC on the surface.

SERS Measurements on Dye Release from Individual AuNCs. The AuNCs loaded with 1-tetradecanol and dye adsorbed on silicon surface were exposed to water in a scintillation vial, which was placed in an oil bath set to 42 °C for different periods of time. Following the incubation for a desired duration, the substrate was cooled in ice-cold water followed by thorough rinsing with nanopure water before drying with a stream of nitrogen. The sparsely deposited AuNCs were identified using an optical microscope under dark-field illumination to obtain SERS spectra of individual AuNCs using a Renishaw InVia confocal Raman spectrometer coupled to a Leica microscope with 50× objective (NA = 0.75). The excitation wavelength used was 785 nm with a laser power of ~4 mW at the sample surface.

UV/Vis/NIR Measurements on Dye Release from the AuNCs by Heating. The 1.5 mL centrifuge tubes containing AuNCs loaded with 1-tetradecanol and dye were placed in an oil bath set to 42 °C and incubated for different periods of time. Following the incubation for a desired duration, the solution was rapidly cooled by immersing into an ice bath for 5 min, followed by centrifugation at 13 000 rpm for 10 min. The absorption of the supernatant was collected using UV−vis spectrometer.

Cell Culture. Human epithelial breast cancer cells (SKBR3) were purchased from ATCC (Manassas, VA) and subcultured in Mc.Coy's 5A medium with 10% fetal bovine serum (FBS) and antibiotics (100 μg/mL penicillin and 100 μg/mL streptomycin) (Sigma, St. Louis, MO). Cells were grown in water jacket incubator at 37 °C with 5% CO_2-humidified atmosphere in 25 cm^2 tissue culture flasks. Once the cells reached to 90% confluence, they were washed with phosphate buffered saline (PBS), detached with 1 mL of 0.25% trypsin-EDTA solution (Sigma), and then redispersed in 10 mL of complete medium. Cells were plated on poly(lysine)-coated silicon substrates placed in a flat-bottom, 24-well plate (Fisher Scientific, Pittsburgh, PA) at a density of 1×10^4 cells over 0.5 cm × 0.5 cm.

***In Vitro* Drug Payload Release Using SKBR3 Cells.** Once the SKBR3 cells plated on silicon substrates reached 90% confluence, they were rinsed twice with PBS and 0.5 mL of AuNCs loaded with nile red in serum-free medium was added. Then, the cells were incubated for 1 h at 37 °C enabling passive internalization. After 1 h, the cells were washed three more times with PBS to completely remove the free and weakly bound AuNCs. Finally, SERS spectra were collected on the monolayer of live cells using 785 nm laser with 20× objective (NA = 0.4).

Electromagnetic Simulations. The spatial distribution of the electromagnetic field intensity around the nanostructures was investigated using a three-dimensional finite-difference time-domain (FDTD) method with commercial software (EM Explorer). FDTD simulations are based on modeling electromagnetic waves behavior by exploiting the time and position dependence of Maxwell's equations in rectangular 3D cells of finite volume (Yee cells). The simulation domain size is 300 nm × 300 nm × 300 nm and contains one cubic shell nanostructure with outer edge length of 80 nm and wall thickness of 6 nm, which is very close with actual geometry of the AuNCs observed with TEM. To obtain the extinction profile, a wavelength scan (400−1100 nm) was performed using p-polarized incident plane wave for illumination, and perfectly matched layer (PML) absorbing boundary conditions were applied in all directions. The electromagnetic field vector and intensity distribution was acquired by performing a high resolution simulation (Yee cell size of 1 nm) at the extinction wavelengths of λ = 710 and 814 nm, and incident excitation wavelength of λ = 785 nm, respectively. Refractive index table of gold is used to set the optical parameters.[53]

Instrumentation. Transmission electron microscopy (TEM) micrographs were recorded on a JEOL JEM-2100F field emission (FE) instrument. Samples were prepared by drying a drop of the solution on a carbon-coated grid, which had been previously made hydrophilic by glow discharge. SEM images were collected using a JEOL JSM-7001 FLV field emission SEM at an accelerating voltage of 15 kV. SERS spectra were collected using a *Renishaw inVia* confocal Raman spectrometer mounted on a Leica microscope in the range of 100−3200 cm^{-1}. UV−vis−NIR extinction spectra were collected using a Shimadzu UV-1800 spectrometer.

Conflict of Interest: The authors declare no competing financial interest.

Acknowledgment. The authors thank Dr. Abdennour Abbas for technical help with FDTD simulations. We acknowledge the financial support from the Office of Congressionally Directed Medical Research Programs under contract No. W81XWH-11-1-0439, and BRIGHT institute at Washington University in St. Louis under P50 Pilot Project Program and Nano Research Facility (NRF), a member of the National Nanotechnology Infrastructure Network (NNIN), for providing access to electron microscopy facilities.

Supporting Information Available: SERS enhancement factor calculation, E-field vectors at five different *X*−*Y* planes of Au nanocage excited at 710 and 814 nm wavelengths, SEM of Au nanocages, EM field of a AuNC. This material is available free of charge *via* the Internet at http://pubs.acs.org.

REFERENCES AND NOTES

1. Maier, M. S. *Plasmonics: Fundamentals and Applications*; Springer: New York, 2007.
2. Ozbay, E. Plasmonics: Merging Photonics and Electronics at Nanoscale Dimensions. *Science* **2006**, *311*, 189–193.

3. Nikolajsen, T.; Leosson, K.; Bozhevolnyi, S. I. Surface Plasmon Polariton Based Modulators and Switches Operating at Telecom Wavelengths. *Appl. Phys. Lett.* **2004**, *85*, 5833–5835.
4. Cai, W.; White, J. S.; Brongersma, M. L. Compact, High-Speed and Power-Efficient Electrooptic Plasmonic Modulators. *Nano Lett.* **2009**, *9*, 4403–4411.
5. Sriturayanich, W.; Pan, L.; Wang, Y.; Sun, C.; Bogy, D. B.; Zhang, X. Flying Plasmonic Lens in the Near Field for High-Speed Nanolithography. *Nat. Nanotechnol.* **2008**, *3*, 733–737.
6. Rontzsch, L.; Heinig, K. H.; Schuller, J. A.; Brongersma, M. L. Thin Film Patterning by Surface-Plasmon-Induced Thermocapillary. *Appl. Phys. Lett.* **2007**, *90*, 044105.
7. Rosi, N. L.; Mirkin, C. A. Nanostructures in Biodiagnostics. *Chem. Rev.* **2005**, *105*, 1547–1562.
8. Maier, S. A.; Atwater, H. A. Plasmonics: Localization and Guiding of Electromagnetic Energy in Metal/Dielectric Structures. *J. App. Phys.* **2005**, *98*, 011101.
9. Anker, J. N.; Hall, W. P.; Lyandres, O.; Shah, N. C.; Zhao, J.; Van Duyne, R. P. Biosensing with Plasmonic Nanosensors. *Nat. Mater.* **2008**, *7*, 442–453.
10. Mayer, K. M.; Hafner, J. H. Localized Surface Plasmon Resonance Sensors. *Chem. Rev.* **2011**, *111*, 3828–3857.
11. Sepulveda, B.; Angelome, P. C.; Lechuga, L. M.; Liz-Marzán, L. M. LSPR-based Nanobiosensors. *Nano Today* **2009**, *4*, 244–251.
12. Dreaden, E. C.; Alkilany, A. M.; Huang, X.; Murphy, C. J.; El-Sayed, M. A. The Golden Age: Gold Nanoparticles for Biomedicine. *Chem. Soc. Rev.* **2012**, *41*, 2740–2779.
13. Dreaden, E. C.; Mackey, M. A.; Huang, X.; Kang, B.; El-Sayed, M. A. Beating Cancer in Multiple Ways Using Nanogold. *Chem. Soc. Rev.* **2011**, *40*, 3391–3404.
14. Bardhan, R.; Lal, S.; Joshi, A.; Halas, N. J. Theranostic Nanoshells: From Probe Design to Imaging and Treatment of Cancer. *Acc. Chem. Res.* **2011**, *44*, 936–946.
15. Xia, Y.; Li, W.; Cobley, C. M.; Chen, J.; Xia, X.; Zhang, Q.; Yang, M.; Cho, E. C.; Brown, P. K. Gold Nanocages: From Synthesis to Theranostic Applications. *Acc. Chem. Res.* **2011**, *44*, 914–924.
16. Cobley, C. M.; Chen, J.; Cho, E. C.; Wang, L. V.; Xia, Y. Gold Nanostructures: A Class of Multifunctional Materials for Biomedical Applications. *Chem. Soc. Rev.* **2011**, *40*, 44–56.
17. Tian, L.; Morrissey, J. J.; Kattumenu, R.; Gandra, N.; Kharasch, E. D.; Singamaneni, S. Bioplasmonic Paper as a Platform for Detection of Kidney Cancer Biomarkers. *Anal. Chem.* **2012**, *84*, 9928–9934.
18. Ko, H.; Singamaneni, S.; Tsukruk, V. V. Nanostructured Surfaces and Assemblies as SERS Media. *Small* **2008**, *4*, 1576–1599.
19. Anker, J. N.; Hall, W. P.; Lyandres, O.; Shah, N. C.; Zhao, J.; Van Duyne, R. P. Biosensing with Plasmonic Nanosensors. *Nat. Mater.* **2008**, *7*, 442–453.
20. Gandra, N.; Singamaneni, S. Bilayered Raman-Intense Gold Nanostructures with Hidden Tags (BRIGHTs) for High-Resolution Bioimaging. *Adv. Mater.* **2013**, *24*, 1022–1027.
21. Abbas, A.; Tian, L.; Morrissey, J. J.; Kharasch, E. D.; Singamaneni, S. Hot Spot-Localized Artificial Antibodies for Label-Free Plasmonic Biosensing. *Adv. Funct. Mater.* **2013**, *23*, 1789–1797.
22. Peer, D.; Karp, J. M.; Hong, S.; Farokhzad, O. C.; Margalit, R.; Langer, R. Nanocarriers as an Emerging Platform for Cancer. *Nat. Nanotechnol.* **2007**, *2*, 751–760.
23. Sailor, M. J.; Park, J. Hybrid Nanoparticles for Detection and Treatment of Cancer. *Adv. Mater.* **2012**, *24*, 3779–3802.
24. Kim, J.; Piao, Y.; Hyeon, T. Multifunctional Nanostructured Materials for Multimodal Imaging, and Simultaneous Imaging and Therapy. *Chem. Soc. Rev.* **2009**, *38*, 372–390.
25. Timko, B. P.; Dvir, T.; Kohane, D. S. Remotely Triggerable Drug Delivery Systems. *Adv. Mater.* **2010**, *22*, 4925–4943.
26. Barreto, J.; Malley, W.; Kubeil, M.; Graham, B.; Stephan, H.; Spiccia, L. Nanomaterials: Applications in Cancer Imaging and Therapy. *Adv. Mater.* **2011**, *23*, H18–H40.
27. Petros, R. A.; DeSimone, J. M. Strategies in the Design of Nanoparticles for Therapeutic Applications. *Nat. Rev.* **2010**, *9*, 615–627.
28. Yezhelyev, M. V.; Gao, X.; Xing, Y.; Al-Hajj, A.; Nie, S.; O'Regan, R. M. Emerging use of Nanoparticles in Diagnosis and Treatment of Breast Cancer. *Lancet Oncol.* **2006**, *7*, 657–667.
29. Weissleder, R. A Clear Vision for *in Vivo* Imaging. *Nat. Biotechnol.* **2001**, *19*, 316–317.
30. Kim, C.; Cho, E. C.; Chen, J.; Song, K. H.; Au, L.; Favazza, C.; Zhang, Q.; Cobley, C. M.; Gao, F.; Xia, Y.; *et al. In Vivo* Molecular Photoacoustic Tomography of Melanomas Targeted by Bioconjugated Gold Nanocages. *ACS Nano* **2010**, *4*, 4559–4564.
31. Yang, X.; Skrabalak, S.; Li, Z.; Xia, Y.; Wang, L. V. Photoacoustic Tomography of a Rat Cerebral Cortex *in Vivo* with Au Nanocages as an Optical Contrast Agent. *Nano Lett.* **2007**, *7*, 3798–3802.
32. Song, K. H.; Kim, C.; Cobley, C. M.; Xia, Y.; Wang, L. V. Near-Infrared Gold Nanocages as a New Class of Tracers of Photoacoustic Sentinel Lymph Node Mapping on a Rat Model. *Nano Lett.* **2009**, *9*, 183–188.
33. Yavuz, M. S.; Cheng, Y.; Chen, J.; Cobley, C. M.; Zhang, Q.; Rycenga, M.; Xie, J.; Kim, C. H.; Song, K. H.; Schwartz, A. G.; *et al.* Gold Nanocages Covered by Smart Polymers for Controlled Release with Near-Infrared Light. *Nat. Mater.* **2009**, *12*, 935–939.
34. Moon, G. D.; Choi, S.-W.; Cai, X.; Li, W.; Cho, E. C.; Jeong, U.; Wang, L. V.; Xia, Y. A New Theranostic System Based on Gold Nanocages and Phase-Change Materials with Unique Features for Photoacoustic Imaging and Controlled Release. *J. Am. Chem. Soc.* **2011**, *133*, 4762–4765.
35. Arcamone, F.; Cassinelli, G.; Fantini, G.; Grein, A.; Orezzi, P.; Pol, C.; Spalla, C. Adriamycin, 14-hydroxydaunomycin, A New Antitumor Antibiotic from *S. peucet* Var. Caesius. *Biotechnol. Bioeng.* **1969**, *11*, 1101–1110.
36. Tan, C.; Tasaka, H.; Yu, K. P.; Murphy, M. L.; Karnofsky, D. A. Daunomycin, an Antitumor Antibiotic, in the Treatment of Neoplastic Disease. Clinical Evaluation with Special Reference to Childhood Leukemia. *Cancer* **1967**, *20*, 333–353.
37. Gosselin, R. E.; Hodge, H. C.; Smith, R. P.; Gleason, M. N. *Clinical Toxicology of Commercial Products*, 4th ed.; Williams and Wilkins: Baltimore, MD, 1976; pp II−118.
38. Skrabalak, S. E.; Au, L.; Li, X.; Xia, Y. Facile Synthesis of Ag Nanocubes and Au Nanocages. *Nat. Protoc.* **2007**, *2*, 2182–2190.
39. Jain, P. K.; El-Sayed, M. A. Universal Scaling of Plasmon Coupling in Metal Nanostructures: Extension from Particle Pairs to nanoshells. *Nano Lett.* **2007**, *7*, 2854–2858.
40. Gandra, N.; Abbas, A.; Tian, L.; Singamaneni, S. Plasmonic Planet-Satellite Analogues: Hierarchical Self-Assembly of Gold Nanostructures. *Nano Lett.* **2012**, *12*, 2645–2651.
41. Lawless, M. K.; Mathies, R. A. Excited-State Structure and Electronic Dephasing Time of Nile Blue from Absolute Resonance Raman Intensities. *J. Chem. Phys.* **1992**, *96*, 8037.
42. Ru, E. C. L.; Schroeter, L. C.; Etchegoin, P. G. Direct Measurement of Resonance Raman Spectra and Cross Sections by a Polarization Difference Technique. *Anal. Chem.* **2012**, *84*, 5074–5079.
43. Malynych, S.; Luzinov, I.; Chumanov, G. Poly(vinyl pyridine) as a Universal Surface Modifier for Immobilization of Nanoparticles. *J. Phys. Chem. B* **2002**, *106*, 1280–1285.
44. Nergiz, S. Z.; Singamaneni, S. Reversible Tuning of Plasmon Coupling in Gold Nanoparticle Chains Using Ultrathin Responsive Polymer Film. *ACS Appl. Mater. Interfaces* **2011**, *3*, 945–951.
45. Rycenga, M.; Wang, Z.; Gordon, E.; Cobley, C. M.; Schwartz, A. G.; Lo, C. S.; Xia, Y. Probing the Photothermal Effect of Gold-Based Nanocages with Surface-Enhanced Raman Scattering (SERS). *Angew. Chem., Int. Ed.* **2009**, *48*, 9924–9927.
46. Wu, E. C.; Park, J.; Park, J.; Segal, E.; Cunin, F.; Sailor, M. J. Oxidation-Triggered Release of Fluorescent Molecules or Drugs from Mesoporous Si Microparticles. *ACS Nano* **2008**, *2*, 2401–2409.
47. Eliasson, C.; Lorén, A.; Murty, K. V. G. K.; Josefson, M.; Käll, M.; Abrahamsson, J.; Abrahamsson, K. Multivariate

Evaluation of Doxorubicin Surface-Enhanced Raman Spectra. *Spectrochim. Acta, Part A* **2001**, *57*, 1907–1915.
48. Lorén, A.; Eliasson, C.; Josefson, M.; Murty, K. V. G. K.; Käll, M.; Abrahamsson, J.; Abrahamsson, K. Feasibility of Quantitative Determination of Doxorubicin with Surface-Enhanced Raman Spectroscopy. *J. Raman Spectrosc.* **2001**, *32*, 971–974.
49. Matousek, P. Deep Non-invasive Raman spectroscopy of Living Tissue and Powders. *Chem. Soc. Rev.* **2007**, *36*, 1292–304.
50. Stone, N.; Faulds, K.; Graham, D.; Matousek, P. Prospects of Deep Raman Spectroscopy for Noninvasive Detection of Conjugated Surface Enhanced Resonance Raman Scattering Nanoparticles Buried within 25 mm of Mammalian Tissue. *Anal. Chem.* **2010**, *82*, 3969–3973.
51. Stone, N.; Kerssens, M.; Lloyd, G. R.; Faulds, K.; Graham, D.; Matousek, P. Surface Enhanced Spatially Offset Raman Spectroscopic (SESORS) Imaging—The Next Dimension. *Chem. Sci.* **2011**, *2*, 776–780.
52. Bergholt, M. S.; Lin, K.; Zheng, W.; Lau, D. P.; Huang, Z. *In Vivo*, Real-time, Transnasal, Image-Guided Raman Endoscopy: Defining Spectral Properties in the Nasopharynx and Larynx. *J. Biomed. Opt.* **2012**, *17*, 077002.
53. Palik, E. D. *Handbook of Optical Constants of Solids*; MA: Academic: Boston, MA, 1985.